Growth-induced self-organization in bacterial colonies

You, Z.

Cover Page

The following handle holds various files of this Leiden University dissertation:
http://hdl.handle.net/1887/74473

Author: You, Z.
Title: Growth-induced self-organization in bacterial colonies
Issue Date: 2019-06-25

Chapter 5

Mono-to-multilayer transition

Previous chapters have shown various examples of emergent phenomena induced by cell growth in expanding monolayers, free or confined. In this chapter, we will demonstrate that in-plane cell growth can also drive an escape to the third dimension, and trigger a transition from mono- to multilayer structure, i.e. the next step toward biofilm formation. Such a mono-to-multilayer transition has recently drawn significant attention in the biophysical literature, being a universal step in biofilm formation, as well as a process where mechanical forces are likely to play a leading role. Grant *et al.* explored the effects of various mechanical forces on the mono-to-multilayer transition in *E. coli* colonies confined between a glass slide and an agarose gel [56]. They measured the transition position and the size of the colony at the onset, from both experiments and simulations, and studied how these quantities were mediated by different mechanical interactions. More recently, Beroz *et al.* [66] demonstrated that, in *V. cholerae* biofilms, the transition is triggered by the mechanical instability of individual cell. Using a mean-field calculation, they find that the critical pressure decreases with the cell length and, consequently, the transition is more likely to be triggered by a cell division. Similar mechanisms are also found in confluent monolayers of eukaryotic cells [110–117, 13, 118] and are believed to regulate cell extrusion and apoptosis. These works have greatly contributed to shed light on the problem, however, a general understanding of the physical mechanisms underpinning the mono-to-multilayer transition is still lacking, with questions far outnumbering the answers so far: *1)* Is there a well-defined critical state? *2)* If so, what determines the critical state? *3)* Can we predict when and where the transition will happen?

In this chapter we address these questions theoretically, using a combination of numerical and analytical methods. We demonstrate that the

mono-to-multilayer transition in a system of growing rod-like cells results from a competition between the in-plane active stresses, that compress the cells laterally, and the vertical restoring forces, owing to the cell-substrate interactions (e.g. compression from the agarose on top or adhesion from the substrate beneath). As the colony expands, the internal stress increases until it is sufficiently large to cause extrusion of the first cell. In the ideal case of a chain-like colony of laterally-confined non-growing cells, being compressed from the two ends, the transition is entirely deterministic and the critical stress that triggers the extrusion can be calculated analytically. Asynchronous cell division, however, renders the transition stochastic. In this case, the critical stress is a continuously distributed random variable and the first extrusion does not necessarily occur at the colony center, despite this being the region of maximal stress. Upon modeling the transition as a Poisson process, we can approximately calculate the probability distribution function (PDF) of the position and time associated with the first extrusion. Finally, we show that rate of the Poisson process, is analogous to an order parameter and that, in this respect, the mono-to-multilayer instability is likened to a continuous phase transition.

5.1   Simplified hard-rod model

We still use the hard-rod model introduced in section 2.1, with suitable simplification of mechanical interactions. Whereas cells in bacterial colonies are potentially subject to a large variety of mechanical and biochemical stimuli, here we focus on three types of forces that are important to the transition: the repulsive forces associated with cell-cell and cell-substrate steric interactions and a vertical restoring force, representing either the mechanical compression from the agarose gel on top [56, 65], or the attractive force due to adhesion of the cells with the glass slide or the ECM [66]. Neighboring cells interact with the same way as shown in section 2.1, with an exception that the forces are now Hookean instead of Hertzian. This can greatly simplify the analysis of mechanical interactions and make analytical treatments possible, while preserving the same physical picture. The force from the jth cell to the ith is then $\boldsymbol{F}_{ij}^c = k_c h_{ij} \boldsymbol{N}_{ij}$, with k_c the elastic constant of cells. Similarly, the force from the substrate is $\boldsymbol{F}_{i\alpha}^s = k_s(d_0/2 - z_{i\alpha})\hat{\boldsymbol{z}}$, where $z_{i\alpha}$ is the $z-$coordinate of the caps, if $z_{i\alpha} < d_0/2$, or $\boldsymbol{F}_{i\alpha}^s = k_a l_i(d_0/2 - z_{i\alpha})\hat{\boldsymbol{z}}$, if $d_0/2 < z_{i\alpha} < d_0/2 + r_a$. Here, k_s and k_a represent respectively the elasticity of the substrate and
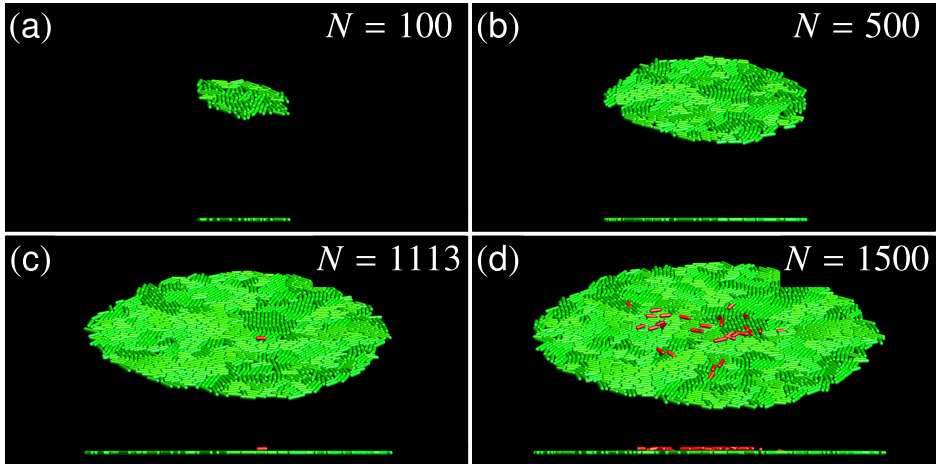
Figure 5.1. Snapshots of a simulated growing colony at different ages to show the mono-to-multilayer transition. The lower image in each panel shows the side view. In panels (c) and (d), the extruded cells are highlighted as red.

the strength of the vertical restoring force, and r_a is the range of the restoring force, beyond which the restoring force vanishes. The vertical restoring force in general can depend on cell length in a very complicated manner. Here, we simply set the vertical restoring force to be proportional to the cell length, which is true in case of cell-substrate adhesion where the number of adhesion molecules is proportional to the area of the cells [66]. We stress that our model does not aim to accurately reproduce the traits of a specific bacterial family, but rather to abstract the essential features that all bacteria undergoing the mono-to-multilayer transition have in common.

We integrate Eqs. 2.2 numerically using the following set of parameter values: $d_0 = 1\,\mu$m, $k_c = k_s = 10$ MPa μm, $\zeta = 100$ Pa h and $r_a = 0.01\ \mu$m[62]. The division length l_d varies from $3\,\mu$m to $4\,\mu$m and the growth rate varies from $1\,\mu$m/h to $2\,\mu$m/h. The integration is performed with a time step $\Delta t = 10^{-6}$ h.

Figure 5.1 shows typical configurations of our *in silico* colonies at different time points. Consistent with the experimental evidence [61, 56], the colony initially expands as a perfect monolayer (Figs. 5.1a,b) and, once it is sufficiently large, some cells are extruded and initiate a second layer (Figs. 5.1c,d).

77

5.2 Mechanics of mono-to-multilayer transition

The mechanical interactions in the full 3D model is very complicated, for the repulsion between neighboring cells depends on their relative position and the relative orientation. For simplicity, we look at a simplified chain-like colony, consisting of a row of cells confined in a channel (Fig. 5.2a). This, in the simulation, is done by manually setting the y components of r_i and p_i to be zero for all cells and at all times. The cells have identical length l and do not grow, but are compressed by a pair of forces f applied at the two ends of the channel. By doing so, we can manually control the internal stress in the colony, hence can accurately determine the critical state at which the transition happens. At the beginning of the simulation, all cells are right on top of the substrate, i.e., $z_i = d_0/2$ and $q_{xi} = 1$. Then the compression force is increased very slowly from $0N$, such that the colony is at mechanical equilibrium for all times. In other words, all cells are experiencing the same internal stress imposed by the compression on the two ends.

As in the case of disk-like colonies (Fig. 5.1), cells remain perfectly attached to the substrate for small compression forces. Once the compression force exceeds a certain value, one of the cells is extruded to the second layer. The existence of a well-defined critical force, f^*, at which the monolayer becomes unstable, indicates that the transition is entirely deterministic in this case. The critical force f^* can be calcu-
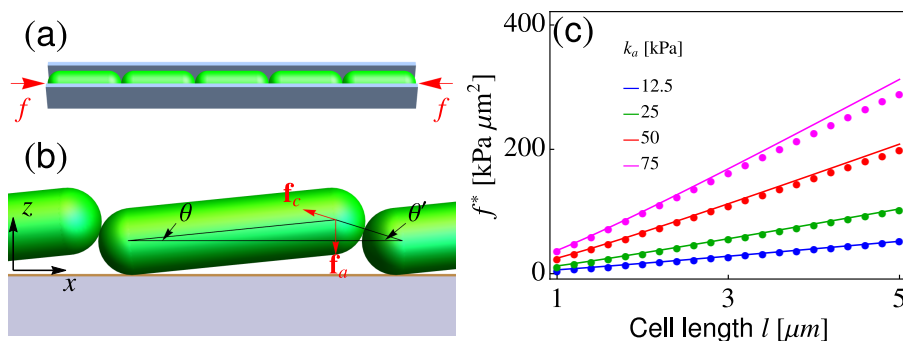
Figure 5.2. (a) Schematic diagram of the chain-like colony. (b) Schematics of torque balance about the lower end of the cell. (c) Critical force f^* as a function of the cell length l, at various k_a values. The dots and lines represent respectively the simulation and analytical results as in Eq. 5.2.

lated analytically upon balancing the torques associated with cell-cell and cell-substrate interactions, about the lower end of the cell axis. Calling $\boldsymbol{p} = (\cos\theta, 0, \sin\theta)$ the orientation of the first extruded cell and $\boldsymbol{f_c} = f_c(-\cos\theta', 0, \sin\theta')$, with $f_c = f/\cos\theta'$, the contact force exerted by the nearby cell (Fig. 5.2b), the lifting torque can be calculated in the form: $\tau_c = l(p_x f_z - p_z f_x) = lf\cos\theta(\tan\theta + \tan\theta')$. Analogously, the restoring torque resulting from the adhesive force is $\tau_a = k_a l^3 \sin\theta\cos\theta$. In a perfectly horizontal monolayer, $\theta = \theta_0 = 0$ and both torques vanish. Any deviation from the equilibrium configuration will induce increases of both torques with respect to θ, at rates

$$\begin{aligned}
\frac{d\tau_c}{d\theta} &\approx fl\left(1 + l/d_0\right) \\
\frac{d\tau_a}{d\theta} &\approx k_a l^3,
\end{aligned}$$

(5.1)

respectively. Note that $d\tau_c/d\theta$ increases linearly with the compression force f. For a sufficiently small f vale, τ_a outgrows τ_c, hence any deviation from the equilibrium configuration, however small it is, will be brought back to balance. This is why the cells are perfectly attached to the substrate when $f < f^*$. In order for such a configuration to be unstable against slight orientational fluctuations, one should have $d\tau_c/d\theta \geq d\tau_a/d\theta$. The equality then sets the critical force as:

$$f^* = k_a l^2 \left(1 + \frac{l}{d_0}\right)^{-1},$$

(5.2)

in excellent agreement with the result of our numerical simulations (Fig. 5.2c). The existence of a well defined critical force resulting from the competition between compression and rotation is vaguely reminiscent of Euler's buckling in elastic rods. However, while buckling is a system-wide instability, the mono-to-multilayer transition is determined by torque balance at the length scale of a single cell.

5.3 Stochastic theory

Next we study the mono-to-multilayer transition in a growing colony. Cells are again confined in the channel for simplicity and, unlike the previous case, they are not subject to lateral compression, but elongate and divide. To investigate the effect of the key parameters, k_a, l_d, and g, we perform

four sets of 10^5 simulations, starting from a single cell at the equilibrium configuration. In the "control" set, we fix $k_a = 25$ kPa, $l_d = 4$ μm, and $g = 2$ μm/h. In each of the remaining three sets we change one of the parameters.
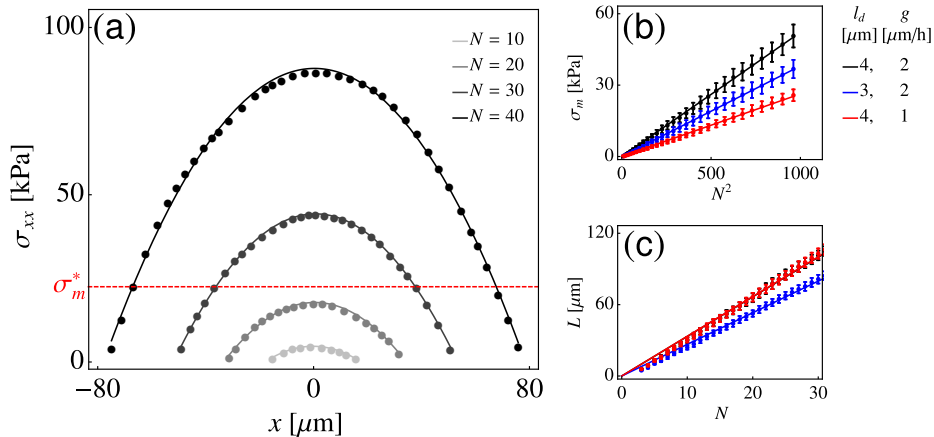
Figure 5.3. (a) The spatial distributions of stress in growing chain-like colonies at different ages, at the "control" parameters. (b) The maximum stress σ_m is proportional to N^2, while (c) the colony length L increases linearly with cell number N. The error bars show the standard deviations of results from 10000 runs about the average values. Solid lines indicate the best fit, linear or parabolic, to the data points.

As the colony expands, the internal stress progressively builds up. To have a quantitative understanding of the spatial-temporal evolution of internal stress, we measure the internal stress experienced by each cell via the virial construction as we did in the previous chapters (see e.g. Refs. [38, 60]). We focus on the in-plane stresses that trigger the mono-to-multilayer transition, namely:

$$\boldsymbol{\sigma}_i = \frac{1}{a_i} \sum_{j=1}^{N_i^c} (\boldsymbol{\Pi} \cdot \boldsymbol{r}_{ij})(\boldsymbol{\Pi} \cdot \boldsymbol{F}_{ij}^c) \, , \qquad (5.3)$$

where $a_i \approx d_0(l_i + d_0)$ is the area of the i-th cell and $\boldsymbol{\Pi} = \boldsymbol{I} - \hat{\boldsymbol{z}}\hat{\boldsymbol{z}}$, with $\boldsymbol{I}$ the identity, is a projection operator on the $xy-$plane. In the case of a chain-like colony, such as that depicted in Fig. 5.2a, the $y-$components of both $\boldsymbol{r}_{ij}$ and $\boldsymbol{F}_{ij}^c$ vanish and σ_{xx} is the only nonzero component of the in-plane stress. Because of the extensile nature of growth-induced stress, σ_{xx}

has negative values. Nevertheless, for convenience, we neglect the sign of σ_{xx}, and use it to indicate the magnitude of the in-plane stress, i.e. $|\sigma_{xx}|$. While the local stress experienced by each cell is increasing with time, at the colony scale it follows a simple parabolic profile of the form:

$$\sigma_{xx}(x) = \sigma_m \left[1 - \left(\frac{2x}{L} \right)^2 \right] , \tag{5.4}$$

where σ_m and L represent respectively the maximum stress and the colony length (Fig. 5.3a). Numerically, we find that $\sigma_m = aN^2$ and $L = bN$ (Figs. 5.3b and 5.3c), where N is the total number of cells and a and b are constants depending only on the division length l_d and the growth rate g.

The stress profile shown in Eq. 5.4 can be derived analytically by assuming an over-damped dynamics and the incompressibility of cells. Consider a cell of length l and position x, subject to a stress difference

$$\Delta\sigma_{xx} = \sigma_{xx}(x + l/2 + d_0/2) - \sigma_{xx}(x - l/2 - d_0/2) \tag{5.5}$$

on the two ends. From Eq. 5.3, the resultant force on the cell is $\Delta F_x = -d_0 \Delta\sigma_{xx}$, and the velocity

$$\begin{aligned}
v_x &= -\frac{d_0}{\zeta l} \Delta\sigma_{xx} \\
&= -\frac{d_0(l + d_0)}{\zeta l} \frac{\Delta\sigma_{xx}}{l + d_0} \\
&\approx -\frac{d_0(l + d_0)}{\zeta l} \frac{\partial\sigma_{xx}}{\partial x} ,
\end{aligned} \tag{5.6}$$

or equivalently

$$\begin{aligned}
\frac{\partial\sigma_{xx}}{\partial x} &= -\frac{\zeta l}{d_0(l + d_0)} v_x \\
&\approx -\frac{\zeta l_a}{d_0(l_a + d_0)} v_x ,
\end{aligned} \tag{5.7}$$

where $l_a = (l_d + l_m)/2$ and $l_m = (l_d - d_0)/2$ are respectively the average and minimal lengths of cells.

Now we will get the velocity profile. Assume the cell chain is symmetric about the point $x = 0$. If the amount of overlap between neighboring cells

is reasonably small compared to the cell length, the velocity of a cell at position $x > 0$ is

$$v_x = \sum_{0 < x_i \le x} g_i \approx \frac{xg}{l_a + d_0}. \tag{5.8}$$

The last approximation is based on the *Law of Large Number*, where $x/(l_a + d_0)$ is the average number of cells in region $(0, x]$. Especially, the total number of cells, on average, is $N = L/(l_a + d_0)$. Hence, parameter b can be approximated as $b \approx (l_a + d_0)$. Substitute Eq. 5.8 in Eq. 5.7, and integrate both sides of the equation from x to $L/2$, we have

$$\int_x^{L/2} \frac{\partial \sigma_{xx}}{\partial x'} dx' = -\int_x^{L/2} dx' \frac{\zeta g l_a}{d_0 (l_a + d_0)^2} x'. \tag{5.9}$$

By applying the boundary condition $\sigma_{xx}(L/2) = 0$, one arrives at

$$\sigma_{xx}(x) = \frac{\zeta g l_a L^2}{8 d_0 (l_a + d_0)^2} \left[1 - \left(\frac{2x}{L} \right)^2 \right]. \tag{5.10}$$

It can be demonstrated that Eq. 5.10 also applies to cells at $x < 0$. Since $L = (l_a + d_0)N$, $\sigma_m = \zeta g l_a N^2/(8 d_0)$ and $a = \zeta g l_a/(8 d_0)$. Comparison between the simulated and analytical values of a and b can be found in Tab. 5.1.

Parameters	b [μm]		a [kPa]	
[μm],[μm/h]	Simulation	Analytics	Simulation	Analytics
$l_d = 3, g = 2$	2.8	3.0	0.038	0.050
$l_d = 4, g = 2$	3.5	3.7	0.052	0.068
$l_d = 4, g = 1$	3.5	3.7	0.026	0.034

Table 5.1. Comparison between the simulated and analytical values of a and b.

Because the stress is maximal at the center of the colony, one would expect the first extrusion to occur here. Our simulations, however, show a dramatically different behavior. Specifically, the position of the first extruded cell x^* has a random value and it follows a broad distribution, whose spread is comparable to the size of the colony itself (Fig. 5.4a). Analogously the transition time t^* (Fig. 5.4b) and the critical stress σ^* experienced by cells at the verge of extrusion (Fig. 5.4c), are continuously distributed random variables.
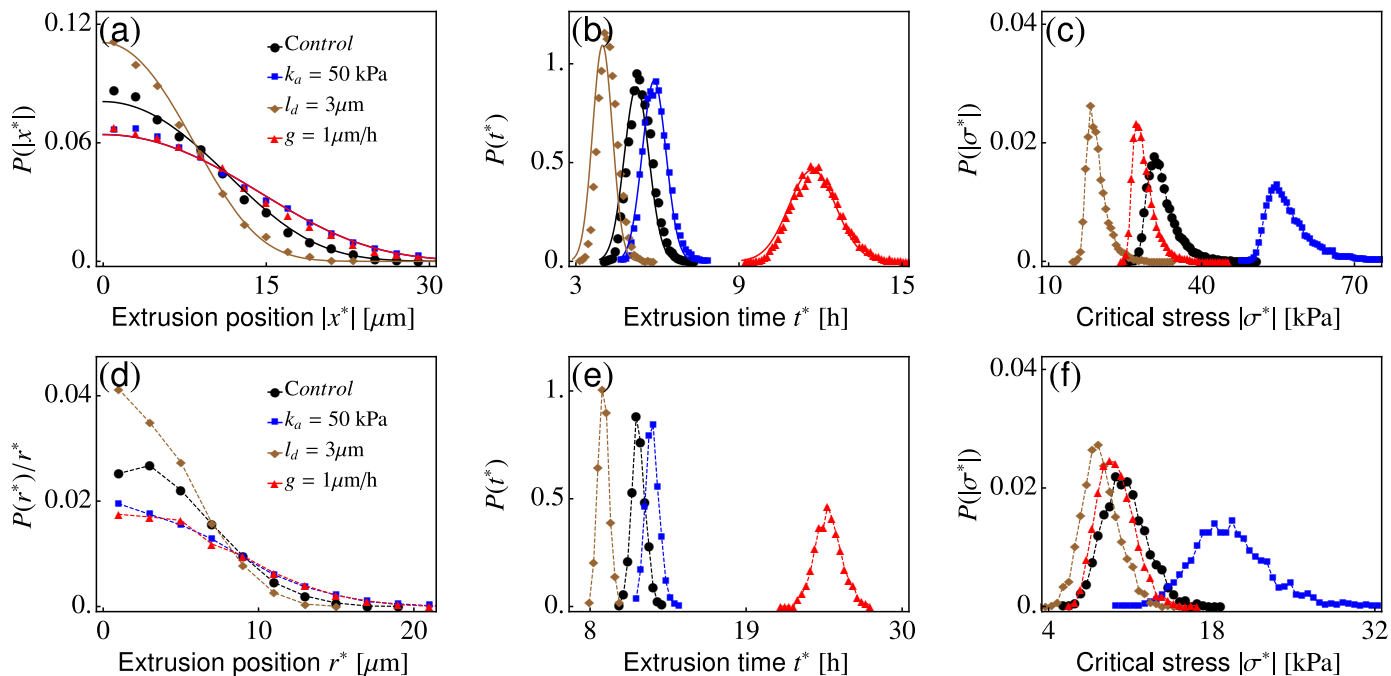
Figure 5.4. (a-c) Probability densities of (a) the extrusion positions $|x^*|$, (b) the extrusion time t^*, and (c) the critical stress σ^*, for chain-like colonies of asynchronously dividing cells. (d) Probability density of the extrusion position r^* in disk-like colonies, normalized by r^*, the distance from the point of extrusion to the centroid of the colony. (e-f) Same as panels (b-c), but for disk-like colonies. In all panels, dots and dashed lines correspond to the simulation results and the solid lines to the analytical predictions. In each set of simulations, one parameter is changed compared to the "control" set, whose parameter values are indicated in the legends. The statistical results for each set of parameters are collected from 10000 runs for chain-like colonies, and 2000 runs for disk-like colonies.

The lack of well defined critical stress is in stark contrast with the classical buckling scenario, but shares some similarity with the onset of fracture in heterogeneous media [119], i.e., the weakest point dominates. In the following, we demonstrate that, in growing bacterial colonies, this behavior results from the combined inherent randomness of cell length and the dependence of critical force on the cell length. According to Eq. 5.2, a cell is unstable to extrusion if subject to a critical stress, whose magnitude increases with the cell length. In a growing colony of desynchronized division, however, cells have different lengths, hence require different critical stresses. In addition, each cell is also experiencing different local stress. This means that the transition can happen to any cell as long as the local stress exceeds the critical stress demanded by the local cell length. As a consequence, there is no unique critical state in a growing colony, but rather an ensemble of them, each corresponding to a specific combination of cell length and the corresponding critical stress. Furthermore, the desynchronization of cell division makes it impossible to predict which critical state to appear first. This is the origin of stochasticity of the mono-to-multilayer transition in a growing bacterial colony.

The stochasticity of the transition demands that the problem can only be tackled with statistical methods. In principle, one can work out the time evolution of the statistical distribution of the critical states, from which the probability distributions of the transition position and time can then be obtained. In practice, we find that the transition is mostly triggered by cell division. This is understandable: a division event introduces a sudden drop in the cell length and this can, in turn, trigger an extrusion instability, as long as the cell is subject to a stress larger than that required to extrude a cell of minimal length $l_m = (l_d - d_0)/2$. A similar phenomenon was found in [66]. We denote such a minimal critical stress σ_m^*. As the stress is spatially inhomogeneous and increasing in time, there will be a whole region, symmetric with respect to the center of the colony and whose length increases in time, where the local stress exceeds σ_m^* and cell division can trigger the first extrusion. We call this region the P-zone. The probability associated with the first extrusion is then equal to the probability of having a division within the P-zone. This can be calculated as follows.

Let us consider a colony of n cells with growth rate g and assume that, at an arbitrary time, their lengths are independent and uniformly distributed in the interval $l_m \leq l \leq l_d$. After a time t, the probability that

no division has yet occurred equates the probability that none of the cells is initially longer than $l_d - gt$:

$$P(t) = \left(\frac{l_d - gt - l_m}{l_d - l_m}\right)^n \approx e^{-\lambda(n)t} , \qquad (5.11)$$

where $\lambda(n) = ng/(l_d - l_m)$ and the approximation holds for large n values ($n \gtrsim 5$). Equation 5.11 defines a Poisson process of rate $\lambda(n)$ [120]. In the case where the cell growth rate is also a random variable uniformly distributed in the interval $g/2 \leq g_i \leq 3g/2$, as we have in our hard-rod model, one can prove the rate to become

$$\lambda(n) = \frac{1}{l_d - l_m} \sum_{i=1}^{n} g_i . \qquad (5.12)$$

For sufficiently large n values, by the *law of large number*, we have $\sum_{i=1}^{n} g_i \approx ng$ so that:

$$\lambda(n) \approx \frac{ng}{l_d - l_m} . \qquad (5.13)$$

Furthermore, if n is time-dependent, the process becomes inhomogeneous, but the probability preserves the same structure, with $\lambda(t) \equiv \lambda[n(t)]$ and $P(t) = e^{-\int_0^t dt\, \lambda(t)}$ [120]. The PDF associated with observing the first division at time t is then:

$$f(t) = \frac{d}{dt}[1 - P(t)] = \lambda(t)e^{-\int_0^t dt'\, \lambda(t')} . \qquad (5.14)$$

In our case, n represents the number of cells within the P-zone. Given the length of the P-zone L^*, the total number of cells in it is a random variable because of the random growth rate. Approximating $\sum_{i=1}^{n} l_i \approx nl_a$ (again, *law of large number*), with $l_a = (l_d + l_m)/2$ the average cell length, we have $n = L^*/(l_a + d_0)$. L^* can be calculated by solving $\sigma_{xx}(L^*/2) = \sigma_m^*$ (red dashed line in Fig. 5.3a). This yields:

$$L^* = b\sqrt{N^2(t) - N_0^2}, \qquad (5.15)$$

where $N_0 = \sqrt{\sigma_m^*/a}$ is the minimal number of cells required for the P-zone to exist. From this and Eq. 5.13, we can calculate the rate $\lambda(t)$ as:

$$\lambda(t) = \frac{gb}{(l_d - l_m)(l_a + d_0)}\sqrt{N^2(t) - N_0^2} \sim [N(t) - N_0]^{1/2} . \qquad (5.16)$$
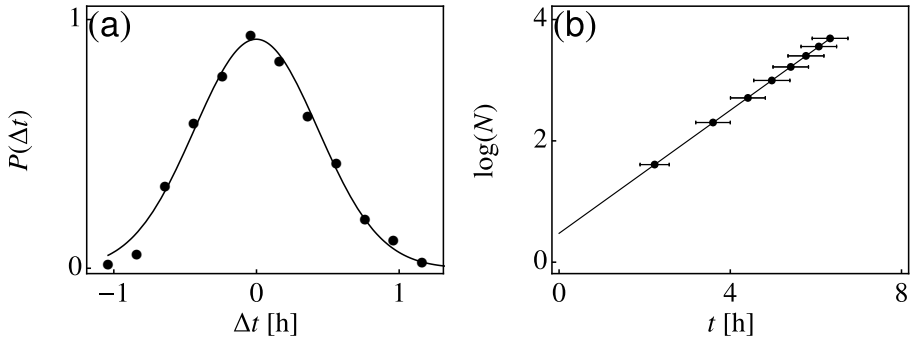
Figure 5.5. Relation between cell number N and time t, at $l_d = 4\mu m$ and $g = 2\mu m/h$. (a) The time t taken by the colony to attain a given population N is a random variable of the form $t = \bar{t} + \Delta t$, with Δt Gaussianly distributed (the solid line shows the best Gaussian fit). (b) N increases exponentially with the average time $\bar{t}$. The black dots represent the average $\bar{t}$ and the horizontal error bars show the standard deviation of 10^4 data samples about the average value $\bar{t}$.

Equation 5.16 highlights the role of λ as an order parameter for the mono-to-multilayer transition. For $N(t) < N_0$, λ is imaginary and the probability of observing an extrusion vanishes identically. On the other hand, for $N(t) > N_0$, λ is real and the probability of observing an extrusion increases in time. The transition is continuous in this case, but other scenarios are likely possible.

To make the time-dependence explicit in Eq. 5.16, we need to calculate $N(t)$. Evidently, the average number of cells in the colony grows exponentially in time. Because of the random growth rate, the time t taken for the colony to attain a given population N is a random variable of the form $t = \bar{t} + \Delta t$. Numerically, we find that Δt follows a Gaussian distribution $\mathcal{N}(0, \delta_{\Delta t}^2)$ with a zero mean and a variance $\delta_{\Delta t}^2$ (Fig. 5.5a). In addition, $N(\bar{t}) \sim \exp(\omega \bar{t})$ (Fig. 5.5b), as a consequence of the exponential growth, or equivalently $\bar{t} = \omega^{-1} \log(N)$. We can then express $t = \omega^{-1} \log(N) + \Delta t$ and $N(t) = \exp[\omega(t - \Delta t)]$. Replacing this in Eq. 5.16 yields:

$$\lambda(t, \Delta t) = \frac{gb}{(l_d - l_m)(l_a + d_0)}\sqrt{e^{2\omega(t-\Delta t)} - N_0^2} \ . \qquad (5.17)$$

As shown in Fig. 5.6, at fixed $\Delta t = 0$, $\lambda(t, 0) \sim \sqrt{t - t_0}$ for $t \gtrsim t_0$, where $t_0 = \omega^{-1} \log(N_0)$ is the average time at which the P-zone first appears. Because of the exponential decreasing of $f(t)$ with increasing λ,
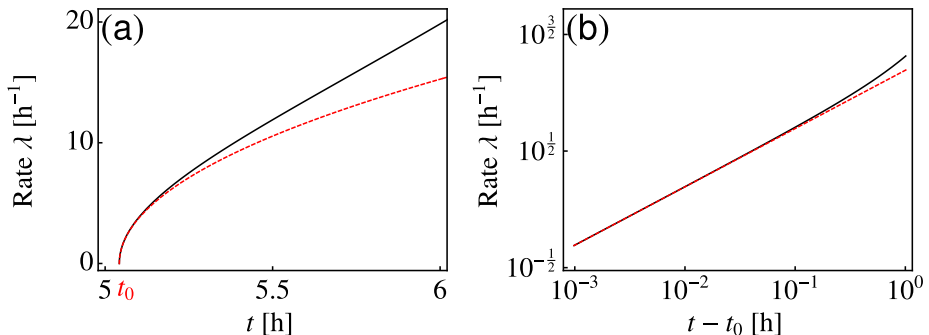
Figure 5.6. (a) Rate $\lambda(t,0)$ (i.e. Eq. 5.17) of the Poisson process at the "control" parameters. (b) Same as panel (a), but in a Log-Log scale. The red dashed lines in both panels show the plots of $\lambda(t,0) = k_\lambda \sqrt{t - t_0}$.

most extrusions happen in this time region. This yields, for nonzero Δt and $t > t_0 + \Delta t$,

$$\lambda(t, \Delta t) \approx k_\lambda \sqrt{t - t_0 - \Delta t}, \tag{5.18}$$

where

$$k_\lambda = \frac{gbN_0\sqrt{2\omega}}{(l_d - l_m)(l_a + d_0)}, \tag{5.19}$$

which can be obtained by Taylor-expanding $\lambda(t, \Delta t)$ about $t_0 + \Delta t$.

The probability distribution function (PDF) associated with observing the first extrusion at time t, given its offset Δt from the average $\bar{t}$, can then be expressed as a conditional PDF of the form:

$$
\begin{aligned}
f(t|\Delta t) &= \lambda(t, \Delta t)e^{-\int_0^t \lambda(t', \Delta t)\mathrm{d}t'} \\
&= k_\lambda(t - t_0 - \Delta t)^{1/2}e^{-\frac{2}{3}k_\lambda(t-t_0-\Delta t)^{3/2}},
\end{aligned}
\tag{5.20}
$$

which is a Weibull distribution and can be approximated as a Gaussian distribution of the same mean and variance [121]:

$$f(t|\Delta t) \approx \mathcal{N}\left[t_0 + \Delta t + \Gamma\left(\frac{5}{3}\right)\left(\frac{3}{2k_\lambda}\right)^{\frac{2}{3}}, \left(\frac{3}{2k_\lambda}\right)^{\frac{4}{3}}\left[\Gamma\left(\frac{7}{3}\right) - \Gamma^2\left(\frac{5}{3}\right)\right]\right]. \tag{5.21}$$

The PDF of the extrusion time t^* can be found, therefore, upon integrating

87

over Δt:

$$p(t^*) = \int_{-\infty}^{\infty} d\Delta t\, f(t^*|\Delta t) \mathcal{N}(0, \delta_{\Delta t}^2)$$

$$= \mathcal{N}\left[t_0 + \Gamma\left(\frac{5}{3}\right)\left(\frac{3}{2k_\lambda}\right)^{\frac{2}{3}}, \left(\frac{3}{2k_\lambda}\right)^{\frac{4}{3}}\left[\Gamma\left(\frac{7}{3}\right) - \Gamma^2\left(\frac{5}{3}\right)\right] + \delta_{\Delta t}^2 \right].$$
(5.22)

As demonstrated by Fig. 5.4b, the analytical results are in good agreement with those obtained from the numerical simulations.

Since cell division occurs uniformly in the P-zone, the PDF associated with observing an extrusion at time t and position x is given by:

$$f(x, t|\Delta t) = \frac{f(t|\Delta t)}{L^*}$$

$$= \frac{\lambda(t, \Delta t)}{L^*} e^{-\int_0^t \lambda(t', \Delta t) dt'},$$
(5.23)

for $-L^*/2 < x < L^*/2$. From Eqs. 5.15 and 5.16, $\lambda/L^* = g/[(l_d - l_m)(l_a + d_0)]$. Substituting this in Eq. 5.23 gives

$$f(x, t|\Delta t) = \frac{g}{(l_d - l_m)(l_a + d_0)} e^{-\int_0^t \lambda(t', \Delta t) dt'}$$

$$= \frac{g}{(l_d - l_m)(l_a + d_0)} e^{-\frac{2}{3} k_\lambda (t - t_0 - \Delta t)^{3/2}}$$
(5.24)

Thus, the conditional PDF associated with observing an extrusion at position x, given the offset Δt, is:

$$f(x|\Delta t) = \int_{t_p(x)+\Delta t}^{\infty} dt\, f(x, t|\Delta t)$$

$$= \int_{t_p(x)}^{\infty} dt'\, f(x, t'|0)$$
(5.25)

$$= f(x|0),$$

where we have used the transformation $t' = t - \Delta t$ and by virtue of Eq. 5.17, $f(t, |\Delta t)$ depends on t and Δt only via the combination $t - \Delta t$. Here, $t_p(x)$ is the average time at which position x first enters the P-zone. From Eq. 5.25, $f(x|\Delta t)$ is independent of Δt. The PDF associated with observ-

ing the first extrusion at position $|x^*|$ is then:

$$
\begin{aligned}
p(|x^*|) &= 2 \int_{t_p(x^*)}^{\infty} \mathrm{d}t \, f(x,t|0) \\
&= \frac{2g}{(l_d - l_m)(l_a + d_0)} \int_{t_p(x^*)}^{\infty} \mathrm{d}t \, e^{-\frac{2}{3}k_\lambda (t-t_0)^{3/2}} \\
&= \frac{2g}{(l_d - l_m)(l_a + d_0)} \left(\frac{2}{3}\right)^{\frac{1}{3}} k_\lambda^{-\frac{2}{3}} \Gamma\left[\frac{2}{3}, \frac{2}{3}k_\lambda \left(t_p(x^*) - t_0\right)^{\frac{3}{2}}\right],
\end{aligned}
\tag{5.26}
$$

where $\Gamma[s,x]$ is the incomplete Gamma function. It can be demonstrated that $[t_p(x) - t_0]^{1/2} = k_x x$, where $k_x = 2/(bN_0\sqrt{2\omega})$. Substitute this in Eq. 5.26, we have

$$
\begin{aligned}
p(|x^*|) &= \frac{2g}{(l_d - l_m)(l_a + d_0)} \left(\frac{2}{3}\right)^{\frac{1}{3}} k_\lambda^{-\frac{2}{3}} \Gamma\left[\frac{2}{3}, \frac{2}{3}k_\lambda k_x^3 x^{*3}\right] \\
&= \left(\frac{2}{3}k_\lambda k_x^3\right)^{\frac{1}{3}} \Gamma\left[\frac{2}{3}, \frac{2}{3}k_\lambda k_x^3 x^{*3}\right],
\end{aligned}
\tag{5.27}
$$

which again agrees well with the simulations (Fig. 5.4a).

Finally, let us go back to the original disk-like colonies. In a disk-like colony, the emergence of nematic domains makes the stress anisotropic,
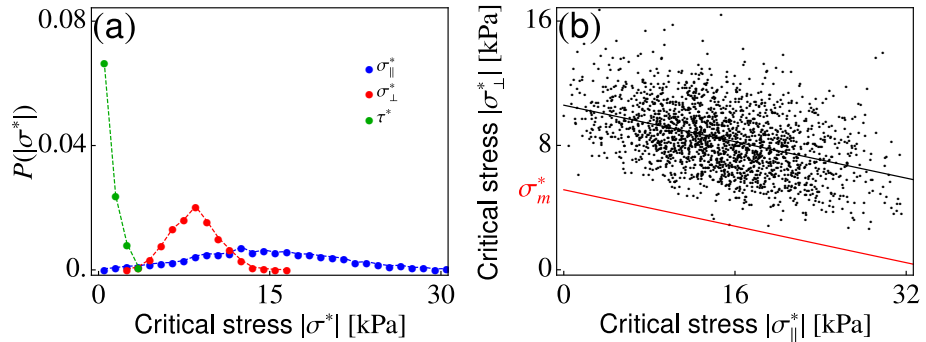
Figure 5.7. Critical stress in a disk-like colony at the "control" parameters. (a) The probability distributions of different components of the critical stress. (b) The two normal components of the critical stress $\sigma_\parallel^*$ and $\sigma_\perp^*$ are anti-correlated (i.e. $\sigma_\perp^* \sim -\sigma_\parallel^*$) and fall above a line of minimal critical stress σ_m^* (in red). The black line shows a linear fit to the data points: $|\sigma_\perp^*| \sim -c|\sigma_\parallel^*|$.

as discussed in chapter 3. The in-plane stress tensor can, nevertheless, be decomposed into longitudinal and transverse components, namely:

$$\boldsymbol{\sigma}_i = \sigma_{i\parallel}\boldsymbol{p}_i^{\parallel}\boldsymbol{p}_i^{\parallel} + \sigma_{i\perp}\boldsymbol{p}_i^{\perp}\boldsymbol{p}_i^{\perp} + \tau_i(\boldsymbol{p}_i^{\parallel}\boldsymbol{p}_i^{\perp} + \boldsymbol{p}_i^{\perp}\boldsymbol{p}_i^{\parallel})\,, \qquad (5.28)$$

where $\boldsymbol{p}_i^{\parallel} = [p_{ix}, p_{iy}]$ and $\boldsymbol{p}_i^{\perp} = [-p_{iy}, p_{ix}]$. To encode the anisotropy of the stress tensor in the transition, we measure the critical stresses of the extruded cells, and extract the three components, whose probability densities are shown in Fig. 5.7a. The shear component τ^* is always negligible, whereas both normal stresses affect the stability of the planar configuration. Specifically, plotting $\sigma_{\parallel}^*$ against $\sigma_{\perp}^*$, we find that the two critical normal stresses are linearly related to each other (Fig. 5.7b), namely: $\sigma_{\perp}^* \sim -c\sigma_{\parallel}^*$, with c a positive constant. In addition, all data points fall above a line with the same slope (red line in Fig. 5.7b). These results indicate that in a planar colony the two normal stresses are working together to extrude cells. In addition, a $\sigma_{\perp}$ can trigger the transition as easily as a $\sigma_{\parallel} = \sigma_{\perp}/c$, and the fact that $c < 1$ means that the amount of contributions from the two normal stresses to the instability of cells are different. The cause for this correlation is still unknown, and requires further investigations of mechanical interactions in the full 3D scenario, which is beyond the scope of this thesis. Nevertheless, based on the results shown in Fig. 5.7, we can define an effective stress $\sigma = \sigma_{\perp} + c\sigma_{\parallel}$ for each cell, as well as a minimal effective critical stress σ_m^* as indicated in Fig. 5.7b. Whenever $\sigma > \sigma_m^*$, a cell division can always trigger a mono-to-multilayer transition. Figures 5.4d-e show the probability distributions of the extrusion position, the extrusion time, and the effective critical stress $\sigma^* \equiv \sigma_{\perp}^* + c\sigma_{\parallel}^*$ for the original disk-like colonies (e.g. Fig. 5.1). Despite the mechanical interactions being more complex in disk-like colonies, the physical picture emerging from the simulations is nearly identical to that discussed for chain-like colonies.

5.4 Discussion and conclusion

The enormous variety of physical and biochemical mechanisms observed in cellular systems defeats the notion of universality, despite this, biofilms and tissues feature traits that are consistently found across several morphotypes and species, such as the capability of transitioning from simple monolayers to more complex multilayered structures [56, 65, 66, 110, 111,

116, 13]. Whereas this transition manifests itself in a multitude of possible variants, depending upon the nature of the environmental and intercellular forces, it robustly relies on a limited number of fundamental principles, which most cellular systems have in common. First, the interplay between steric interactions and active motion or growth, drives the formation of coherent structures on the plane, such as nematic domains [122], topological defects [13] or large groups of collectively moving cells [30]. Second, the extensile stresses arising from the in-plane spatial organization and the lack of vertical confinement, drives the cellular layer to be unstable to extrusion. Because intercellular forces are mainly repulsive, this process occurs at the scale of individual cells, in spite of the collective origin of the in-plane stresses driving the instability. Third, the transition is both deterministic and stochastic. For a given configuration of the colony, there is well defined critical stress, related with the cells *local* arrangment (e.g. cell length and nematic order). But, as this is inherently random, so is the critical stress and, consequently, the extrusion time and position. Therefore, there is no uniquely defined critical state, but rather an ensemble of them. Upon modeling cell division as a Poisson process, and under the assumption that newly divided cells are the first to be extruded, we were able to reconstruct the probability distribution of the extrusion time and position for a simple laterally-confined chain-like colony, finding excellent agreement with our numerical data. The rate λ of the Poisson process is analogous to the order parameter in phase transitions and, as the transition depends on the details of the system uniquely via λ, we expect our result to be generic and carry over to other systems, as long as λ can be derived or approximated.